KTH Chemical Science and Engineering

Tailoring adhesion and wetting properties of cellulose fibers and model surfaces

Emil Gustafsson

Licentiate thesis

School of Chemical Science and Engineering
Department of Fibre and Polymer Technology
Wallenberg Wood Science Center and Fibre Technology

KTH Royal Institute of Technology

Stockholm, Sweden 2012

AKADEMISK AVHANDLING
som med tillstånd av Kungliga Tekniska Högskolan i Stockholm
framlägges till offentlig granskning för avläggande av teknologie licentiatexamen
19 mars 2012, kl. 14.00 i K1, Teknikringen 56, KTH, Stockholm
Avhandlingen försvaras på engelska.

Tailoring adhesion and wetting properties of cellulose fibers and model surfaces

Emil Gustafsson

Thesis for the degree of Licentiate of Technology in Fibre and Polymer Science

KTH Royal Institute of Technology
School of Chemical Science and Engineering
Department of Fibre and Polymer Technology
Wallenberg Wood Science Center
SE-10044 Stockholm, Sweden

ISBN 978-91-7501-268-1
TRITA-CHE Report 2012:8
ISSN 1654-1081

Printed by: Universitetsservice US-AB, Stockholm 2012

Abstract

The layer-by-layer (LbL) technique was used to modify the surface of cellulose fibers by consecutive adsorption of poly(allylamine hydrochloride) (PAH) and poly(acrylic acid) (PAA) followed by a final adsorbed layer of anionic paraffin wax colloids. Paper hand sheets made from the modified fibers were found to be highly hydrophobic with a contact angle of 150°. In addition to the significantly increased hydrophobicity, the sheets showed improved mechanical properties, such as a higher tensile strength. Heat treatment of the prepared sheets further enhanced both the mechanical properties and the hydrophobicity. These results demonstrate the flexibility and robustness of the LbL technique, which allows us to combine the known adhesive effect of PAH/PAA LbL films with the functionality of wax nanoparticles, creating a stronger and highly hydrophobic paper.

It was further observed that LbL modified sheets without wax also displayed increased hydrophobicity when heat treated. The mechanism was studied through model experiments where LbL films of PAH/PAA were assembled on flat non-porous model cellulose surfaces. Contact angle measurements showed the same trend due to heat treatment of the model films, although, the absolute value of the contact angles were smaller. Analysis using the highly interfacial sensitive vibrational sum frequency spectroscopy technique showed an enrichment of CH_3 groups (from the polymer chain ends) at the solid/air interface. These results indicate that during the heat treatment, a reorientation of polymer chains occurs to minimize the surface energy of the LbL film.

In the second part of this work, the adhesive interactions between the main constituents of wood fibers were studied using high-resolution measuring techniques and well-defined model films of cellulose, hemicellulose and lignin. Successful surface modification of polydimethylsiloxane (PDMS) caps, needed in the Johnson-Kendall-Roberts (JKR) measuring methodology, by LbL deposition of nanofibrillated cellulose (NFC) and poly(ethylene imine) (PEI) allowed for the first known all-wood biopolymer JKR measurements of the adhesion between cellulose/cellulose, cellulose/lignin and the cellulose/glucomannan surfaces. The work of adhesion on loading and the adhesion hysteresis were similar for all three systems, suggesting that adhesion between the different wood biopolymers does not differ greatly.

Sammanfattning

Layer-by-layer (LbL) tekniken har använts för att ytmodifiera cellulosafibrer genom växelvis adsorption av poly(allylamin hydroklorid) (PAH) and poly(akrylsyra) (PAA) följt av adsorption av ett lager med anjoniska vaxkolloider. Pappersark tillverkades av de modifierade fibrerna och dessa ark fanns vara hydrofoba, med en kontaktvinkel på 150°. I tillägg till den signifikant förbättrade hydrofobiteten uppvisade arken även förbättrade mekaniska egenskaper. Värmebehandling av arken förbättrade både styrkan och hydrofobiteten. Resultaten demonstrerar robustheten och flexibiliteten hos LbL-tekniken genom att visa att styrkeförbättrande polyelektrolyter kan kombineras med vaxpartiklar för att skapa starka papper som samtidigt är hydrofoba.

Vidare observerades det att LbL modifierade ark även utan adsorberat vax blev hydrofoba när de värmebehandlades. Mekanismen bakom detta fenomen studerades vidare genom att cellulosamodellytor modifierades med PAH/PAA för att sedan värmebehandlas. Kontakvinkelmätningar på dessa modellytor visade att ytorna blev mer hydrofoba om än inte i samma utsträckning som de värmda arken. Mekanismen undersöktes vidare med hjälp av vibrational sum frequency spectroscopy (VSFS) och resultaten visade att värmebehandling ger en ökad andel CH_3-grupper på ytan och även signalen för polymerens ryggrad ökade i intensitet. Resultaten indikerar att värmebehandlingen leder till omorientering av polymerkedjorna i LbL-filmen för att minimera ytenergin.

I den andra delen av det här arbetet studerades adhesionsarbetet mellan väldefinierade modellytor av de huvudsakliga vedpolymererna. PDMS-halvsfärer ytmodifierades genom LbL-deponering av nanofibrillerad cellulosa (NFC) och polyetylenimin (PEI) för att skapa en halvsfärisk modellyta av cellulosa. Detta möjliggjorde de första adhesionsmätningarna mellan cellulosa/cellulosa, cellulosa/glukomannan och cellulosa/lignin med Johnson-Kendall-Roberts (JKR) metoden. Adhesionsarbetet och hysteresen för mätningarna skiljde sig inte signifikant för de olika systemen, vilket föreslår att adhesionen mellan de olika vedpolymererna inte skiljer sig markant.

List of publications

I **Treatment of cellulose fibres with polyelectrolytes and wax colloids to create tailored highly hydrophobic fibrous networks**
E. Gustafsson, P.A. Larsson and L. Wågberg
Submitted

II **Vibrational sum frequency spectroscopy on polyelectrolyte multilayers – modeling of hydrophobic fibres**
E. Gustafsson, J. Hedberg, P.A Larsson, L. Wågberg and C.M. Johnson
Submitted

III **Direct adhesive measurements between wood biopolymer model surfaces**
E. Gustafsson, E. Johansson, L. Wågberg and T. Pettersson
Submitted

The contribution of the author of the thesis to the appended papers are:

I All experiments on model surfaces, 50% of the writing
II All sample preparation, AFM, contact angle determinations, major part of the writing
III 50% of the experiments, 50% of the writing

Contents

1 Objectives

The overall objective of the present work has been to identify new routes to molecularly tailor the wetting and adhesive properties of cellulose fibers. This overall objective was divided into three different studies where both cellulose fibers and model surfaces of cellulose, lignin and hemicelluloses were used.

The purpose of **papers I** and **II** was to create a highly hydrophobic paper without any deterioration in the mechanical properties of the paper by using the layer-by-layer (LbL) technique with a combination of polyelectrolytes and nanoparticles of wax.

In **paper III**, the objective was to develop a suitable cellulose model surface deposited on elastic PDMS in order use the Johnson-Kendall-Roberts (JKR) approach to examine the work of adhesion between well-defined model surfaces of wood biopolymers. The purpose of the study was to seek a fundamental understanding of interactions both within the fiber wall and in the fiber-fiber joints in paper.

2 Introduction

2.1 Adhesion

Adhesion science is the science describing how surfaces adhere. Covering all length scales, from the assembly of construction materials to cell adhesion and the interaction of pigments down to the nanoscale interaction between molecules, adhesion phenomena are highly relevant and a great challenge in engineering, chemistry and biology. The thermodynamic work of adhesion upon separation of two surfaces theoretically depends solely on the interfacial energy of the two surfaces and can be predicted by the Dupré equation [1]. The adhesion measured in practice however usually is a non-equilibrium irreversible process in which phenomena like surface roughness, plastic deformation, and molecular reorientation give rise to adhesion hysteresis and real adhesion energies which are orders of magnitude greater than the thermodynamic work of adhesion [1]. It is challenging to measure and decouple these contributions, and if done properly it can provide an important tool towards the tailoring of adhesive interactions and the improvement of material properties.

2.2 Paper and fiber networks

2.2.1 Adhesion in paper and fiber networks

Paper is a three dimensional network of fibers, the overall strength of which depends on the strength of the individual fibers, the fiber length, the number of fiber-fiber joints per volume and the strength of the fiber-fiber joints. Depending on the type of paper, the different factors vary in relative importance. It has been suggested by a theoretical analysis that the maximum tensile strength of a paper ultimately depends on the strength of the individual fibers [2], but it has also been suggested that the adhesive strength of the individual fiber-fiber joints is always the limiting factor for the maximum strength [3]. Without a doubt, it can be stated however that adhesion plays a very important role when it comes to papermaking and that the understanding and tailoring thereof can have large implications for paper applications. The adhesion between fibers and matrix material is also of crucial importance for the performance of fiber-reinforced biocomposites, a material branch that has gained a lot of interest due to the environmental driving force for new, renewable materials.

The dry adhesion between two fibers, i.e. the strength of the fiber-fiber joint, depends on the contact area between the fibers and on the molecular interactions in the contact zone. Traditionally, the adhesion between cellulose fibers is improved by the mechanical treatment of the fibers, so-called “beating”, in order to make the fibers more flexible and to create fibrillar fines [4], both of which contribute to increasing the contact area in the fiber-fiber joint. There are drawbacks of the method though; including impaired dewatering on the paper machine, densification of the paper and high energy consumption.

An alternative to beating is the use of chemicals, usually water-soluble cationic polyelectrolytes, which improve the joint strength without densification. It is well established that the addition of polyelectrolytes increases the molecular contact area and/or the number of fiber-fiber joints [5]. Cationic starch is the most commonly used dry strength additive, primarily due to its low cost, but synthetic polymers such as polyethylenimine (PEI) are also

used [6]. Recently it has been demonstrated that the sequential deposition of oppositely charged polyelectrolytes by the so-called layer-by-layer (LbL) assembly technique can further improve paper strength [7]. LbL assembly also allows for the incorporation of charged nanoparticles, which opens up further possibilities of tailoring fiber and fiber-fiber joint properties. This approach is used in this work and will be further outlined in later sections of this thesis.

2.2.2 Water interactions in cellulose fiber materials

One of the major drawbacks when comparing paper to e.g. plastics is its sensitivity to both liquid water as and moist air. Commonly used paper grades are protected from liquid water by hydrophobation, or sizing. Traditionally this is done by treating the fibers with rosin sizes and alum (acidic sizing), or by adsorbing Alkyl Ketene Dimer (AKD) wax or alkenylsuccinic anhydride waxes (alkaline sizing) prior to sheet forming to make the paper hydrophobic [8]. With AKD sizing, it is possible to achieve advancing contact angles of water of approximately 110° [9]. To reach higher degrees of hydrophobicity however, not only are other methods and/or chemicals needed, but also the introduction of a structured surface in the micrometer range [10, 11].

The wetting of a fibrous material such as paper is complex since it has a chemically and physically heterogeneous surface. The problem is further complicated by the simultaneous spreading of the liquid on the surface and absorption of the liquid into the pores of the material.

When a drop of liquid is placed on a surface, the drop appears to adopt a constant shape with an angle towards the surface which is called the contact angle, θ. The equilibrium contact angle is considered to be a characteristic of the particular liquid-solid interaction and serves as an indication of the wettability of the surface by the liquid. This equilibrium situation for a smooth, homogeneous, impermeable and non-deformable surface is described by the Young equation:

$$\gamma_{sv} = \gamma_{sl} + \gamma_{lv} \cos\theta \qquad (1)$$

where θ is the contact angle of the liquid at the solid-liquid-vapor boundary γ_{sv} is the surface tension of the solid, γ_{lv} is the surface tension of the liquid and γ_{sl} is the interfacial tension between the solid and the liquid.

However, most real surfaces do not have the ideal characteristics which allow the Young equation to be used in its original form. The main reasons, which are certainly the case for wood fibers and paper, are surface roughness and heterogeneity. The experimentally observed contact angle is called the apparent contact angle and if inserted into Young's equation the result will only be approximate. Furthermore, on very thin films the test liquid can diffuse through the film and the measured contact angle may thus be influenced by the interfacial properties of the underlying substrate.

The contact between a liquid and a rough surface can adopt two states; either the liquid is in complete contact with the solid surface or the drop rests on a composite surface of solid and

air. The relation between the apparent contact angle on a rough surface (θ^*), the roughness coefficient (r) and the intrinsic contact angle (θ) has been described by the Wenzel equation:

$$\cos\theta^* = r\cos\theta \quad (2)$$

and by the Cassie-Baxter equation:

$$\cos\theta^* = f_1\cos\theta - f_2 \quad (3)$$

where f_1 is the surface area of the liquid in contact with the solid divided by the projected area, and f_2 is the surface area of liquid in contact with the trapped air divided by the projected surface area.

These equations suggest that there are two basic ways of improving the hydrophobicity of a surface; (a) by lowering the surface energy, and b) increasing the surface roughness, i.e. increasing the surface area, on a meso- and microscopic scale [10-13]. In addition to the effect of microscopic roughness, the hydrophobicity of a surface can be further increased by the introduction of additional roughness on the nanometer scale [14].

2.3 Tailoring of surfaces by the layer-by-layer (LbL) technique

The layer-by-layer (LbL) technique for modifying the surface of charged solid substrates by the consecutive adsorption of polyelectrolytes or charged nanoparticles was introduced as a general method by Decher in the 1990s [15]. The technique, by which polyelectrolyte multilayers (PEM) are formed, has since developed rapidly as a robust, flexible and environment friendly surface engineering technique and notable applications include contact lens coatings [16], sensor technology [17], antibacterial fibers [18] and hollow capsules for the controlled release of drugs [19].

The principle is that when a polyelectrolyte is adsorbed to the surface it recharges the surface, after which the surface is rinsed to wash away unadsorbed or loosely adsorbed polyelectrolytes, followed by the adsorption of an oppositely charged polyelectrolyte and yet another rinsing step. This procedure is repeated until the desired thickness is reached. The adsorption is entropy-driven by the counter ions that are released from the surface during the adsorption resulting in an increase in entropy. LbL deposition can be performed by spin-coating, spraying or most commonly by dipping [16]. The properties of the LbL film and the thickness of the adsorbed layers can be tuned by varying one or several parameters during the LbL process. If a weak polyelectrolyte, i.e. where the degree of dissociation of the polymer chain is dependent on pH, is used, the polyelectrolyte conformation can be tuned by varying the pH. In addition to the charge of the polyelectrolytes, the salt concentration, type of salt, molecular weight and temperature influence the properties of the PEM [16].

Wågberg successfully applied the LbL technique to engineer the surface properties of cellulose fibers in order to improve paper strength [7] and since then the relationships between adsorption, film properties and paper strength have been examined [20, 21]. Even though tensile tests on paper provide only indirect information about the adhesive strength of the fiber-fiber joints, the results obtained strongly indicate that the LbL technique improved the fiber-fiber joint-strength. The influence of PAH/PAA multilayers on the adhesion in the

fiber joint have also been evaluated using fiber crosses, the results indicating an increased joint strength [5]. The adhesion between PEMs under wet conditions, typical of those when fiber-fiber joints are formed, has also been studied using colloid probe atomic force microscopy (AFM). The influences of molecular weight, number of layers and polyelectrolyte in the outermost layer were examined [22]. Although these measurements give information about the adhesion in the wet state they do not provide any information about the effect of the drying of the fiber joint.

Lately, several research groups have started to utilize the potential of the surface charge and nano-dimensions of nanocellulose (NFC,CNC) and have started to include fibrils and nanocrystals as a component in LbL assembly, to produce coatings [23-25], and freestanding films [26] and this technique has been applied in this work as cellulose model surfaces for interaction studies.

LbL assembly has also been used to prepare hydrophobic coatings. Glinel [27] showed that charged wax particles could be incorporated as a barrier that protects the polyelectrolytes from liquid water. Zhai et.al [28] used another route where LbL assembly was used to combine polyelectrolytes and silica nanoparticles to create the porous and rough template needed to create a superhydrophobic surface. Contact angles greater than 90° have also been reported for water on cellulose fibers modified by LbL assembly of polyallylamine (PAH) and polyacrylic acid (PAA), provided the cationic polyelectrolyte was in the external layer [29]. The contact angle of water on films assembled from these polyelectrolytes on flat substrates has meanwhile been reported to be 40-50° [30, 31]. The structural or surface chemistry reason for the observed discrepancy has yet to be resolved. Vibrational sum frequency spectroscopy (VSFS) is an interfacial sensitive spectroscopic method that can provide information about the molecular composition at the solid/air interface of a material. In the current work vibrational sum frequency spectroscopy (VSFS) has been used to study the molecular composition at the solid/air interface of LbL films on glass substrates, to study the connection between interfacial chemistry and wettability of the films.

2.4 Wood biopolymer model systems for evaluating adhesion and wetting

There are several high resolution methods available for the direct measurement of adhesive forces between solid substrates, including the surface force apparatus (SFA) [32], colloid probe AFM [33] and a variety of devices for adhesion measurements based on the Johnson-Kendall-Roberts (JKR) theory [34-36] In this work, a JKR device has been used for fundamental studies of the interaction between wood biopolymers. Adhesion measurement according to the standard JKR approach used in this work does not provide any information about the influence of the drying process on the joint strength. A JKR based technique for performing such measurements is however being developed in our laboratory.

A major challenge when it comes to the measurement of adhesion in real engineering situations, including papermaking and the design of biocomposites, is that they involve heterogeneous surfaces that are both chemically and structurally ill-defined. Such surfaces are ill-suited for studies using the above mentioned techniques, since all the methods, in order to permit conclusions relating to molecular-scale mechanisms, require substrates that are smooth

and chemically well-defined. A common approach is to use neat or gently surface modified silica or mica, which have a low surface roughness and permit controlled surface modifications, as model surfaces. In this work, sufficiently smooth and chemically homogeneous, wood biopolymer model films were prepared and characterized and ultimately used for direct adhesive measurements using the JKR-technique.

Various procedures to prepare more advanced model surfaces representing the three main wood components, cellulose, hemicellulose and lignin, are described in the literature [24, 37]. Earlier work on cellulose model surfaces has been based mostly on the spin-coating of regenerated cellulose dissolved in mixtures of N-methylmorpholine-N-oxide (NMMO) and dimethylsulfoxide (DMSO) [38] or lithium chloride/ dimethyldiacetamine (LiCl/DMAc) [39]. Spin-coated surfaces have also been prepared from suspensions of cellulose nanocrystals (CNC) [40] and nanofibrillated cellulose [41]. CNC and NFC have also been used in LbL assembly together with cationic polyelectrolytes to form model surfaces [23, 42]. The morphology and crystallinity vary depending on the starting material and preparation technique [24]. Cellulose model films have also been prepared by LbL assembly and such films terminated with a layer of NFC were the main cellulose model surfaces used for adhesion measurements in the present work. NFC consists of native cellulose I and also contains both crystalline and paracrystalline regions, and this makes it a good cellulose model surface [24]. The fibrilar structure obtained when assembling the films also resembles that of the cellulose fiber.

The interaction between cellulose surfaces in water has been studied using SFA [43] and colloidal probe AFM [44-47] and two comparative studies have demonstrated that the preparation technique used, which determines the surface charge and roughness, was crucial for the cellulose interactions [47, 48]. The interactions between surfaces coated with LbL films containing NFC [24] and CNC [49] in water have been investigated.

Lignin model surfaces were first prepared in the early 1970s [50] and since then surfaces have been prepared using various lignin sources, with different routes for the isolation of the lignin and by different surface preparation techniques. Norgren [37] recently prepared smooth, stable lignin model surfaces by the spin-coating of kraft lignin dissolved in an aqueous alkaline solution. These surfaces were later used for interaction studies between lignin and cellulose in water at various salt concentrations [46] and for wetting studies, where it was shown that the lignin was partially wetted by water. Spin-coated surfaces have recently also been produced from milled wood lignin [51]. The lignin model surfaces in the present work were prepared from a commercial kraft lignin, Indulin AT.

Hemicelluloses occur in different amounts in wood and, depending on the wood species different hemicelluloses are dominating. In softwood, hemicelluloses from the galactoglucomannan (GGM) family are predominant [52]. There are two different GGMs, one galactose-rich type that is soluble in water and one galactose-poor type called glucomannan (GM) that is insoluble in water. The model surfaces of hemicellulose examined in the present thesis were made from glucomannan. In the literature, surface interaction studies involving

hemicellulose model surfaces are rare, but one recent study examined the interaction between xyloglucan grafted onto gold and a cellulose sphere using colloid probe AFM [53].

In addition to providing information about the interactions in the fiber-fiber joints, the wood biopolymer model surfaces described above can be used to study the fundamental interactions within the fibers. The fibers now found in trees and annual plants are the result of an evolutionary process that has created an intricate chemistry and advanced nano- and mesostructures to optimize the fiber properties, for which both fiber structure and chemistry are crucial. The interactions between the wood biopolymers have a profound effect on the mechanical properties of the fibers. However, we possess limited fundamental understanding of the importance of the adhesive interactions between the various chemical constituents of the fiber wall, and this motivates adhesion studies using well-defined model surfaces representing these wood components.

3 Experimental

This chapter presents the key experimental details of this work. For further details the reader is referred to **papers I-III** and the references therein.

3.1 Materials

3.1.1 Substrates

The fibers used throughout this work were an unbeaten, once-dried, virgin softwood kraft pulp (SCA, Östrand Mill, Sweden) bleached according to a (OO)Q(OP)(ZQ)(PO)-sequence. Before use, the pulp was washed and the carboxyl groups of the fibers were converted to their sodium form according to an earlier described procedure [54].

Dissolving grade pulp from Domsjö Fabriker (Örnsköldsvik, Sweden) was used for the preparation of regenerated cellulose II model surfaces. The pulp was extracted with acetone before use.

Polished silicon wafers with a natural oxide layer of 1.4-1.7 nm, were purchased from MEMC Electronic Materials SpA (Novara, Italy). The surfaces were cleaned thoroughly with milli-Q water and ethanol, blown dry with nitrogen and finally plasma-cleaned for 2 min at 30 W (PDC-002 plasma cleaner; Harrick Scientific Inc., Pleasantville, USA). Microscope glass slides were cleaned in a similar manner.

PDMS (Dow Sylgard 182 silicone elastomer kit, base and curing agent) was purchased from Dow Corning (Midland, USA). Droplets of degassed 10:1 mixture of base and catalyst were placed onto hydrophobated glass to form semi-spherical PDMS caps with a typical radius of 1.1 mm. The size of each individual PDMS cap used in the experimental series was measured. The caps were cured at 100 °C for 1 h and were thereafter extracted in heptane for 12 h in a Soxhlet equipment in order to remove unreacted monomer. Flat slabs of PDMS were also prepared in a glass mold, supported by a silicon wafer using the same proportions of base and catalyst.

3.1.2 Chemicals

Poly(allylamine hydrochloride) (PAH; Mw = 15000 g mol^{-1}) and poly(acrylic acid) (PAA; Mw = 7000 mol^{-1}) were purchased from Sigma-Aldrich (Munich, Germany). Poly(ethylene imine) (PEI; Mw = 60000 g mol^{-1}, 53% aqueous solution) was obtained from Acros Organics (Geel, Belgium). Anionic paraffin wax, Ultralube E-340, was purchased from Keim-Additec Surface Gmbg (Kirchberg, Germany). The wax colloids were of commercial grade with a melting temperature of 56–58 °C according to information provided by the supplier. The polyelectrolytes and wax were used without further purification.

Anionic nanofibrillated cellulose (NFC) was prepared at Innventia AB (Stockholm, Sweden) according to a method described earlier [23, 55]. In brief, the NFC was prepared from a commercial sulfite softwood dissolving pulp (Domsjö Dissolving Plus, Domsjö Fabriker, Örnsköldsvik, Sweden) using high-pressure homogenization similar to a previously described method [56], but with carboxymethylation [57] pretreatment of the fibers. The carboxylated nanofibrils had a typical diameter of 5-15 nm and a length of up to 1 µm [23].

Commercial kraft lignin, Indulin AT, was obtained from MeadWestvaco (Richmond, USA) and was purified according to a procedure previously described by Norgren et al. [37]. To remove carbohydrates, the lignin was dissolved in a dioxane:water mixture (9:1) and stirred for 2 h at room temperature. The solution was then centrifuged and the residue, containing undissolved carbohydrates, was removed. The dioxane was thereafter evaporated in a rotavapor and the lignin was freeze-dried. To remove extractives, the freeze-dried lignin was subjected to pentane extraction for 8 h. The number average molecular weight of Indulin AT has previously been determined to be M_n = 1062 mol^{-1} with a polydispersity index of 5.18 using size exclusion chromatography [58].

Glucomannan from Norway spruce (Picea abies) wood holocellulose was extracted with NaOH/H3BO4 and precipitated with Fehling reagent [59]. The precipitate was washed with deionized water, dissolved in 1 M HCl, and further precipitated and washed with ethanol. The purified glucomannan was composed of galactose, glucose, and mannose in a <0.1:1:3.5 ratio and the degree of polymerization, DP, as determined using size exclusion chromatography, was 150.

Methyl iodide was obtained from Acros Organics (Geel, Belgium) and glycerol from Sigma Aldrich (Munich, Germany). Both chemicals were of analytical grade and were used as received.

All other chemicals (hydrochloric acid, sodium hydroxide, sodium chloride and sodium bicarbonate) were of analytical grade.

All solutions were prepared in mill-Q purified water with a resistivity of 18.2 MΩ cm (Synergy 185, Millipore, Bellerica, USA)

3.2 Methods

3.2.1 LbL formation

The bleached fibers were consecutively treated with PAH and PAA according to a method described earlier [7]. The adsorption was performed in a 4 g/L suspension with a background salt concentration of 0.01 M NaCl. Amounts of 30 mg/g fiber were added in each adsorption step. In brief, the cationic PAH was added to the fiber suspension and allowed to adsorb for 20 min. The water with the excess polyelectrolyte was filtered off and the fiber pad was rinsed with water. The pad was then re-suspended and the PAA was added and allowed to adsorb for 20 min, followed by filtering and washing. The procedure was repeated until 2.5 bilayers of polyelectrolyte (PAH/$PAA_{2.5}$) had been added. PAH and PAA were adsorbed at pH 7.5 and 3.5 respectively to optimize the adsorption [20].

LbL films were formed on cellulose model surface substrates by hand-dipping when there were only a few layers or by using a dipping robot (StratoSequence VI, nanoStrata Inc., Tallahassee, USA) according to the same pH strategy and electrolyte concentrations as for the deposition on fibers. The adsorption time for each polyelectrolyte was 10 min followed by 3x2 min rinsing in Milli-Q water. The films were dried with nitrogen gas following the last deposition step.

3.2.2 Handsheet formation and sheet evaluation

Sheets with an average grammage of 100 g/m^2 were prepared using tap water with the aid of a Rapid Köthen handsheet former (Paper Testing Instruments, Pettenbach, Austria). The sheets were dried at 93 °C under a reduced pressure of 95 kPa for 15 min. Some of the PEM-treated sheets were cut in half, and one half of each sheet was further heat-treated for 30 min at 160°C to induce cross-links in the multilayer structure and thus to increase the tensile strength of the sheets [5, 60], and allowing both a spreading of the adsorbed wax on the surface and a fusing with the PEM [27].

Sheets were conditioned at 23 °C and 50% RH, after which the sheet grammage (mass per unit area) was determined and dry tensile testing was performed according to the ISO 1924-3 Standard. The paper strength is presented as the tensile index, which is the maximum tensile force at paper breakage per unit width and unit grammage of the paper. Sheet thickness and density were evaluated by measuring the structural thickness according to a method developed at STFI (now Innventia AB) [61].

3.2.3 Wood biopolymer model surfaces

Cellulose I model surfaces were prepared on silicon oxide and PDMS by LbL assembly of PEI and NFC. An initial layer of PAH was adsorbed followed by 1.5 bilayer of NFC/PEI. The adsorption time for PAH and PEI was 10 min, NFC was allowed to adsorb for 20 min. Three rinsing steps, each of two minutes, were included between the adsorption steps.

A KW-4A spin coater (Chemat Technology, Northridge, USA) was used to prepare model surfaces of NFC in **paper I** and of lignin and glucomannan in **paper III**. Lignin and glucomannan were dissolved in NH_3 at concentrations 1 wt% and 2 wt% respectively for 24 h and thereafter filtered through 0.45-µm polyethersulfone membrane syringe filters. The solutions were thereafter spin-coated onto cleaned silicon oxide substrates at 2000 rpm for 60 s. Cellulose model surfaces were prepared by spin coating from a 0.1 wt% solution of carboxymethylated NFC onto cleaned silicon oxide surfaces at 1500 rpm for 15 s followed by 3500 rpm for 30 s.

3.2.4 AFM imaging and scratch height analysis

The surface morphology of the flat model surfaces and LbL-modified films was imaged using a Nanoscope IIIa AFM (Veeco Instruments, now Bruker AXS, Santa Barbara, USA) with a type E piezoelectric scanner. Images were acquired in tapping mode in air using RTESP Si cantilevers (Bruker Probes, Camarillo, USA) with a nominal resonance frequency of 300 kHz and a typical spring constant of 40 N m^{-1}. In **paper III,** AFM was also used to determine the film thickness by means of digital image analysis of scratched surfaces using the AFM software (Nanoscope version 6.13, Veeco Instruments). The thickness was calculated from the difference between the height of the film and the height of the underlying silicon oxide surface.

3.2.5 JKR adhesion measurements

The adhesion measurement protocol used in this work, where adhesion is measured using surface functionalized soft PDMS hemispherical caps, is based on the JKR contact mechanics theory [62] and was developed in the early 1990s by Chaudhury and Whitesides [35]. In a

typical experiment, an elastic hemispherical PDMS cap is pressed stepwise towards a flat surface placed on a balance. Since the cap is transparent, the contact area between the surfaces can be monitored using a light microscope connected to a CCD camera. The cap is pressed in finite steps against the flat surface and at each step the system is allowed to equilibrate for 10 min. The load and the contact area are recorded at the end of the equilibrating period. The surfaces are loaded until a trigger value of 0.25 g is recorded, at which point the surfaces are unloaded again in the same stepwise manner until the cap and the flat surface are completely separated.

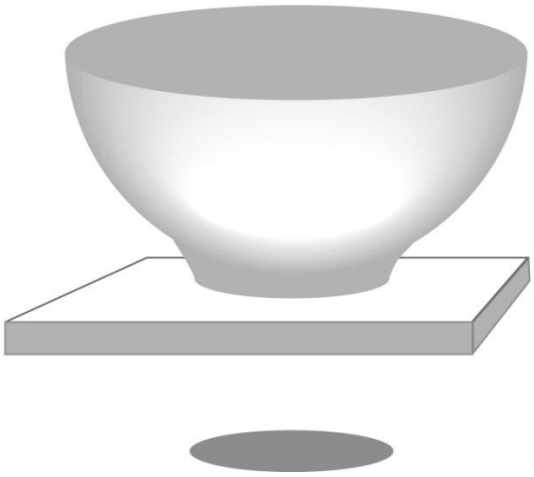

Figure 1.. Illustration of the contact between a hemispherical PDMS cap and a flat surface. The grey area is the projected contact area. Illustration by Mats Rundlöf, AB Capisco Science & Art.

According to the JKR theory, the cube of the contact radius (a^3) and the applied load (F) can be related to the work of adhesion (W) between the cap and the flat surface according to,

$$a^3 = \frac{R}{K}\left[F + 3\pi WR + \sqrt{6\pi WRF + (3\pi WR)^2}\right] \quad (4)$$

where K is the elastic constant for the system and R is the equivalent radius. For cap/flat geometry R equals the radius of the cap which in this work was typically 1.1 mm.

The adhesion energy at minimum load, W_{min}, can be calculated according to

$$F_S = \frac{3}{2}\pi R W_{min} \quad (5)$$

where F_s is the maximum pull-off force obtained from the unloading data.

3.2.6 Contact angle determinations

Static contact angles were determined using Milli-Q purified water, methyl iodide, and glycerol on model surfaces of cellulose $(PAH(NFC/PEI)_{1.5})$, glucomannan and lignin using a KSV CAM 200 goniometer (KSV Instruments, Helsinki, Finland). The surface energy of the model surfaces was calculated from the contact angles according to the method of van Oss[63], which splits the surface energy into a dispersive ,γ^d, and a polar component consisting of acid ,γ^+, and base ,γ^-, contributions.

$$\frac{(1+\cos\theta)\gamma_l}{2} = \sqrt{\gamma_s^d \gamma_l^d} + \sqrt{\gamma_s^- \gamma_l^+} + \sqrt{\gamma_s^+ \gamma_l^-} \quad (6)$$

where γ_l is the surface tension of the liquid and γ_s is the surface energy of the sample.

The method requires a minimum of three test liquids, of which one must be water, since the equation contains three unknowns. In the present work water, methylene iodide, and glycerol were used as test liquids, and the surface tensions, including dispersive, acid, and base components, were taken from Della Volpe [64].

The contact angle for water was also used to determine the effect of surface modifications and heat treatment of surface modified paper sheets and model surfaces.

3.2.7 Vibrational Sum Frequency Spectroscopy (VSFS)

The VSFS spectrometer has been described in detail elsewhere [65]. In brief, an Ekspla (Vilnius, Lithuania) Nd:YAG picosecond laser with an output wavelength of 1064 nm was used to pump an optical parametric generator/optical parametric amplifier (OPG/OPA) from Laservision (Bellevue, USA). A tuneable infrared beam and a visible beam (532 nm) were generated in the OPG/OPA. The output energy from the OPG/OPA in the CH region (2750–3100 cm^{-1}) was approximately 300 µJ. The scanning speed for the infrared beam was 1 cm^{-1}/s. A Spectrogon filter was used at the output of the OPG to remove residual reflections of unwanted frequencies.

4 Results and discussion

4.1 Improved paper strength and hydrophobicity by LbL and wax adsorption

4.1.1 Polyelectrolyte- and wax adsorption on fibers

The LbL assembly technique was used to modify fibers in 4 g fiber/L suspension. PAH and PAA were added at a concentration of 30 mg/g fiber and adsorbed at pH 7.5 and 3.5 respectively with a background electrolyte concentration of 10 mM. These conditions have previously been found to maximize the thickness of the LbL film on the fibers [20]. A layer of anionic paraffin wax particles was adsorbed following the deposition of the final PAH layer. The addition of three different wax concentrations, 3, 15 and 30 mg/g fiber, was evaluated. The particle size distribution of the anionic paraffin wax colloids used was characterized in the pH range between 7.5 – 9.5, with and without the addition of 0.01 M NaCl, by dynamic light scattering. Figure 2 shows a well-defined size distribution and importantly it can also be noted that no particle agglomeration was induced by changes in pH or salt concentration. Furthermore Mütek titrations showed that the charge density was constant within the pH interval 7.5-8.5 and that the presence of salt had only a small influence on the charge density. Wax particles were adsorbed onto the fibers at pH 8.5.

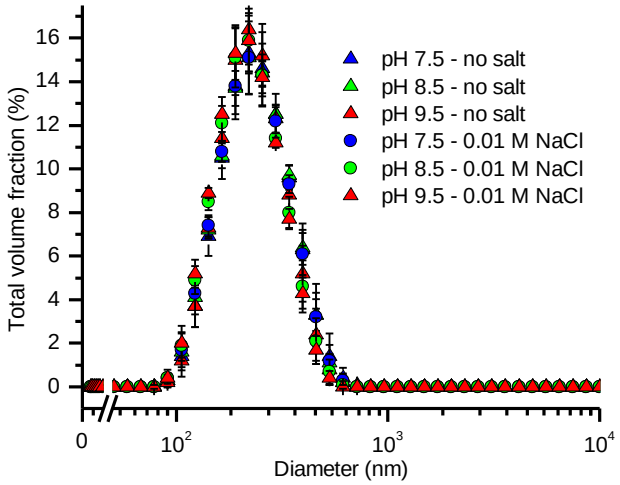

Figure 2. Wax particle size distribution in emulsions of pH 7.5, 8.5 and 9.5 without added NaCl and with an added background NaCl concentration of 0.01 M. The bars indicate 95% confidence limits.

The adsorption of PAH, PAA and wax onto the fibers was determined via titration of non-adsorbed polyelectrolytes from each consecutive step and by extraction of the non-adsorbed wax in the filtrates. As shown in figure 3, the polyelectrolyte adsorption increased for each adsorbed layer and after five layers a total amount of about 75 mg/g fiber had been adsorbed. The wax adsorption was 0.4, 8.1 and 18.6 mg/g for addition of 3, 15 and 30 mg/g fiber added respectively.

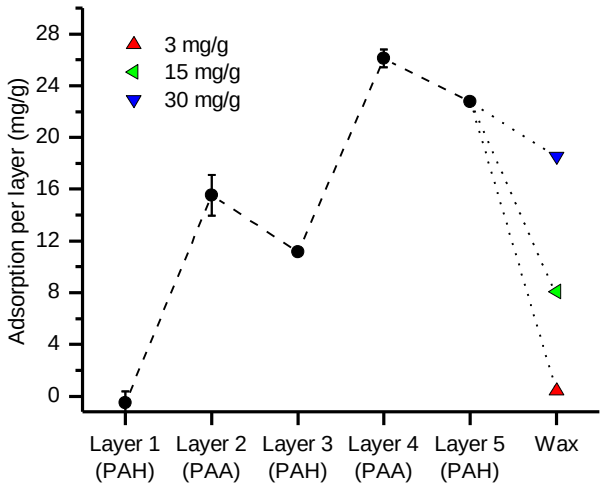

Figure 3. Adsorption analysis via titration of non-adsorbed polyelectrolytes and extraction of adsorbed wax. 95% confidence limits indicate the uncertainty of the titrations.

4.1.2 Sheet formation and mechanical characterization

Handsheets were formed from the surface-modified fibers with the aid of a Rapid Köthen sheet former. After sheet preparation, half the sheets were heat treated for 30 min at 160°C to induce cross-links in the multilayer and thus to increase the strength of the sheets [5, 60] and to allow the adsorbed wax to spread and fuse into the LbL film [27].

LbL formation of $(PAH/PAA)_{2.5}$ on the fibers significantly improved the strength of the hand-sheets, i.e. both tensile strength and strain at break increased (Figure 4). This is in agreement with earlier investigations of the LbL treatment of fibers [7, 20, 66, 67]. Adsorption of wax however led to a reduction in the improved tensile strength as well as in the strain at break. Figure 5 also shows that the modifications had very little effect on the tensile stiffness and density of the sheets.

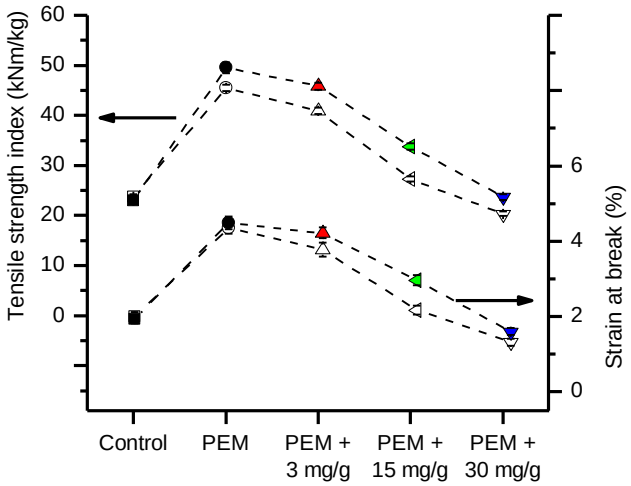

Figure 4. Tensile strength index and strain at break of sheets with five polyelectrolyte layers followed by the addition of wax particles (in mg/g fiber) before sheet forming. Filled symbols indicate samples heat-treated for 30 min at 160 °C, and open symbols indicate samples without any extra heat-treatment. The bars indicate 95% confidence limits.

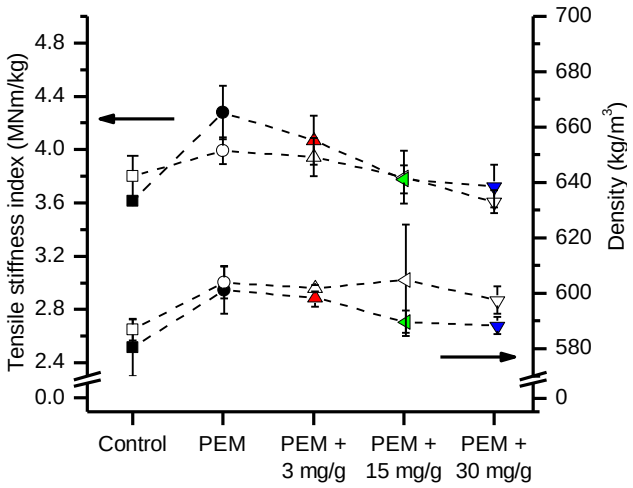

Figure 5. Tensile stiffness index and density of sheets with five polyelectrolyte layers followed by the addition of wax particles (in mg/g fiber) before sheet forming. Filled symbols indicate samples heat-treated for 30 min at 160 °C, and open symbols indicate samples without any extra heat-treatment. The bars indicate 95% confidence limits.

The increase in strength observed for the LbL-modified sheets is interpreted as being a result of an increase in the molecular contact area in the fiber-fiber joints, combined with a greater molecular adhesion in the contact zone due to the intermixing of polymers at the interface [5, 22]. The adsorption of wax colloids partly removed the positive effect of the LbL modification; probably due to the formation of a thin wax layer on top of the PAH/PAA film. This layer has a low surface energy with poor interaction across the interface and may block the migration of molecules from the LbL film across the interface [22]. The heat curing of the sheets led to a further improvement in the paper strength, for both the wax-treated fibers and the LbL-treated fibers without wax addition (Figure 4). This heat-induced improvement in the mechanical properties has previously been reported for PAH/PAA modified fibers by Eriksson [20] and is assigned to a crosslinking reaction within the PEM by amide linkages between the amino groups on the PAH and the carboxyl groups of the PAA, as outlined by Harris [60]. Furthermore an increase in temperature increases the mobility of the polymer chains in the multilayer and this could presumably enhance the intermixing and thus result in a stronger adhesion between the PAH/PAA-modified fibers. Since the adsorption of wax particles led to a deterioration in the improved mechanical properties of the PAH/PAA LbL film, the paper strength in this combined polyelectrolyte/wax colloid system depended on the amount of wax added i.e. the more wax the lower the degree of interpenetration between the polymer layers. However the net effect of the LbL film and the highest wax addition was a sheet with tensile properties similar to those sheets made from the non-treated fibers.

4.1.3 Wetting properties of the sheets

The purpose of the incorporation of wax colloids was to produce a hydrophobic paper and the wetting properties of the sheets were therefore quantified by means of static contact angle determinations. From the contact angles presented in Table 1, the success of the approach is obvious, since the adsorption of wax colloid completely changed the wetting behavior of the resulting sheet. For the sheets with no extra heat treatment, wax adsorption changes the paper from being highly hydrophilic, rapidly absorbing the water drop, to being highly hydrophobic,

enabling the drop of test liquid to rest on the surface with a contact angle as large as 142°. Heat treatment of the wax-containing sheets increased the contact angle further, an increase that is assumed to be a result of a better spreading of the wax. A larger contact angle was achieved when more wax was adsorbed onto the fibers but reached a plateau at approximately 150° with the addition of 15 mg/g fiber, corresponding to an actual adsorption of 8.5 mg/g fiber (Figure 3). At higher wax loads, no further increase in contact angle was achieved but the strength of the sheet decreased drastically (Figure 4).

Table 1. Average contact angle (°) of six drops given with 95% confidence limits, 60 s after applying the droplet onto paper sheets made from the PEM and PEM/wax treated fibers.

	Adsorbed wax (mg/g)	No extra heat treatment	Heat treated
PAH/PAA	0	Absorbing	113 ± 3
PAH/PAA + 3 mg/g	0.4	121 ± 3	122 ± 2
PAH/PAA + 15 mg/g	8.1	138 ± 2	151 ± 3
PAH/PAA + 15 mg/g	18.6	142 ± 2	146 ± 3

The three dimensional network of micrometer wide fibers gives the paper an inherent surface roughness on the micrometer scale. Non-modified cellulose fibers have a high surface energy and are thus highly hydrophilic, resulting in a paper that rapidly absorbs water. When an LbL film is adsorbed on top of the fibers followed by the adsorption of a low surface energy paraffin wax, this changes the surface energy of the fiber network. The result is a rough paper surface consisting of wax-coated fibers with a low surface energy, as indicated by the large contact angle for water on the wax-modified fibers. It has previously been shown using electron microscopy that an LbL assembly of PAH and PAA on wood fibers results in a smooth fiber surface on the micrometer scale [17], therefore, no dramatic change in surface morphology was expected. Furthermore, a qualitative examination of the wax-treated fibers by SEM (results not shown) showed no obvious qualitative increase in roughness, further strengthening the conclusion that the main mechanism behind the increase in hydrophobicity due to the adsorbed wax was by a reduction in the surface energy. However, it cannot be excluded that roughness on a sub-micron scale, from the complex like build-up of the initial layers of PAH/PAA multilayers as suggested by Fujita [38] could enhance the hydrophobicity.

4.1.4 Heat-induced hydrophobation of PAH/PAA films without wax addition

An important result in Table 1, yet to be explained, is that heat-treated sheets made from $(PAH/PAA)_{2.5}$-coated fibers became hydrophobic even without the addition of wax. The hydrophobicity of these heat-treated sheets was also maintained when the surface was wetted by water drops, with no visible penetration into the sheet after 60 s. In fact, the drop rested on the surface until it evaporated or slowly diffused into the paper [68]. This is intriguing given the absorbant nature of the non-heat-treated sheets. The contact angle before heat treatment of the sheets made from PAH/PAA-treated fibers was impossible to measure by the static sessile drop method since the sheet immediately absorbed the drop. This clearly demonstrates the

hydrophilicity of the sheets not exposed to the additional heat treatment. It should be noted, however, that by single fiber measurements using a Cahn balance, Lingström [29] also showed contact angles larger than 90° also for non-heat-treated PAH/PAA-treated fiber, indicating the hydrophobic potential of PAH/PAA LbL films on non-smooth substrates.

To explore the mechanisms of the increase in hydrophobicity upon heat-treatment, $(PAH/PAA)_{2.5}$ were assembled on smooth model surfaces. Silicon oxide surfaces were used as well as two different spin-coated NFC and regenerated cellulose model surfaces. For spectroscopic evaluation of the molecular composition at the solid/air interface, films were also assembled on transparent microscope glass slides. The PAH/PAA films were assembled by dipping the model substrates into polyelectrolyte solutions at 120 mg/L with 10 mM NaCl background electrolyte. A total of 2.5 bilayers were adsorbed, similar to the LbL formation on fibers. Half the surfaces were then heat-treated for 30 min at 160°C. The results of the contact angle determinations, presented in Table 2, show that the $(PAH/PAA)_{2.5}$ film was hydrophilic on all three substrates with a contact angle of about 40°. These values are in reasonable agreement with the 47° previously measured by Choi [31] for a PAH-terminated LbL film of PAH/PAA assembled on a silicon oxide substrate at pH 7.5/3.5. This contact angle is however higher than that measured on cellulose surfaces [69] indicating that the assembly of the PAH-terminated LbL film lowers the surface energy compared to that of the native cellulose fiber. The contact angles measured on flat model films are however in agreement with the hydrophilicity observed for the non-heat-treated paper sheets.

Table 2. Average contact angle (°) of four drops given with 95% confidence limits, 30 s after applying the drop. Heat treatment 160°C for 30 min for 2.5 bl films.

Model system	No extra heat treatment	Heat treated
$(PAH/PAA)_{2.5}$ on NMMO cellulose	22 ± 1	58 ± 1
$(PAH/PAA)_{2.5}$ on NFC	38 ± 1	63 ± 2
$(PAH/PAA)_{2.5}$ on SiO_2	40 ± 1	72 ±1

Table 2 shows that heat treatment of the model films resulted in a distinct increase in the contact angle to a value ranging between 60° and 70°. This increase is suggested to be the result of a reorientation where more hydrophobic groups of the polymer are oriented to the solid-air interface of the system in order to minimize the energy of the surface. This would be possible since the charges of the polyelectrolytes are neutralized during PEM formation [6] and an increase in temperature increases the mobility within the layers and permits an orientation of the alkane chain of the polyelectrolytes towards the surrounding air.

To investigate the proposed change in surface chemistry of the PAH/PAA film due to molecular rearrangements during the heat treatment, the interfacial sensitive spectroscopy technique VSFS was used. Contact angle determinations were performed on the same substrates to compare the change in wetting behavior with the composition of the molecules at the air/solid interface. Slightly thicker films were prepared compared to the previous LbL assemblies in order to ensure a better surface coverage of the substrate and to make sure that

there was a solid bulk of PAH/PAA beneath the surface layer. $(PAH/PAA)_{7.5}$ films were assembled on silicon oxide wafers and on glass slides. The use of glass slides was motivated since VSFS measurements are preferably carried out on transparent substrates in order to reduce the influence of the non-resonant background which makes the interpretation of the spectra more difficult. The samples in this study were heat treated for 90 min at 160°C and in argon atmosphere to prevent contamination.

The results of the contact angle determinations are presented in Figure 6 and, in agreement with the measurements on $(PAH/PAA)_{2.5}$ on fibers and the flat cellulose model surfaces, the $(PAH/PAA)_{7.5}$ films became less hydrophilic after heat treatment. The values were similar on the silicon oxide and glass substrates, and the contact angles were also in good agreement with those measured on $(PAH/PAA)_{2.5}$ film, indicating that the film thickness had little influence on the static contact angle.

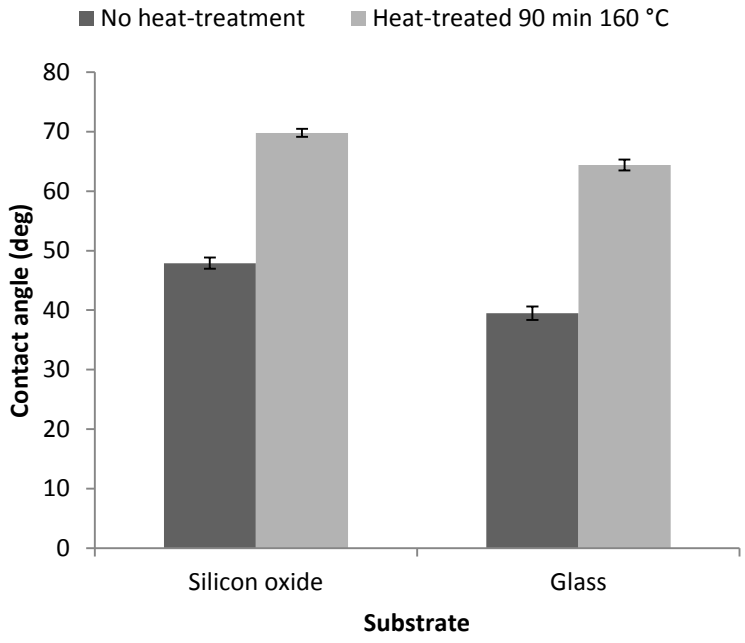

Figure 6. Average water contact angle (°) of 4 drops on heat treated and reference samples of $(PAH/PAA)_{7.5}$ assembled on silicon oxide and glass substrates. The bars indicate 95 % confidence limits.

As previously mentioned, one possible explanation for the increase in contact angle upon heating is that a change in surface morphology is responsible for the decrease in hydrophilicity. No clear change in the surface morphology could however be detected on the scale viewed by SEM and to obtain a higher resolution image of the surface morphology and seek possible changes due to heat treatment, AFM imaging was carried out on the $(PAH/PAA)_{7.5}$ before and after heat treatment. Figure 7 shows some cluster-like features on the film, but no significant change in morphology as a result of the heat-treatment could be detected. The quantitative measure of the rms surface roughness also supported this conclusion, the values being 16 and 12 nm respectively for the non-heated and heated film.

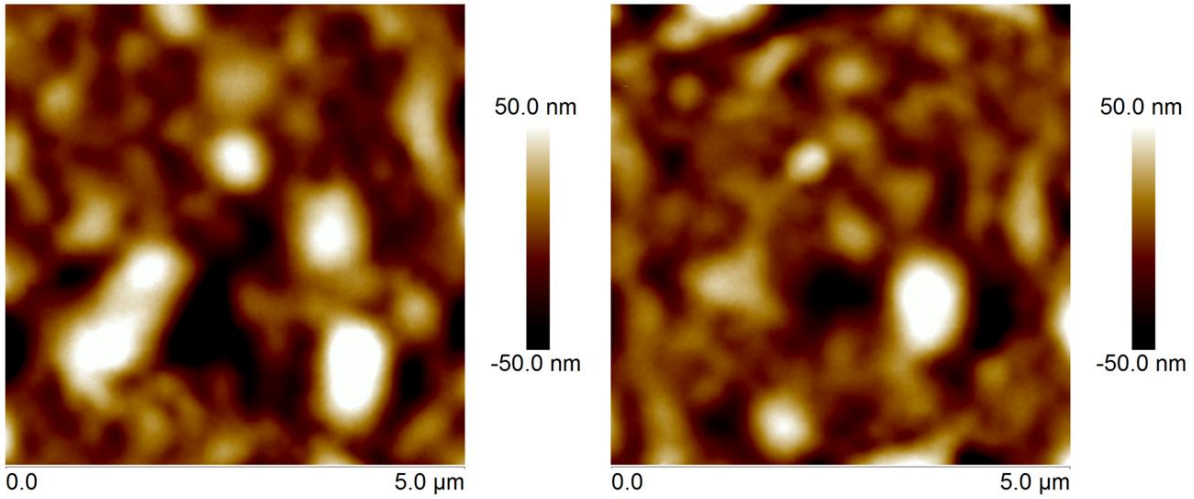

Figure 7. Tapping Mode AFM images of $(PAH/PAA)_{7.5}$ on silicon oxide. Left image displays a film that was not heat treated. The right surface was heat treated for 90 min at 160°C.

Figure 8 shows the VSF spectra of $(PAH/PAA)_{7.5}$ on glass, with and without heat treatment. The measurements were conducted in a pure nitrogen atmosphere in order to minimize the risk of contamination. Two different VSFS active polarization combinations (SSP and PPP) were employed in order to assist in the spectral assignments.

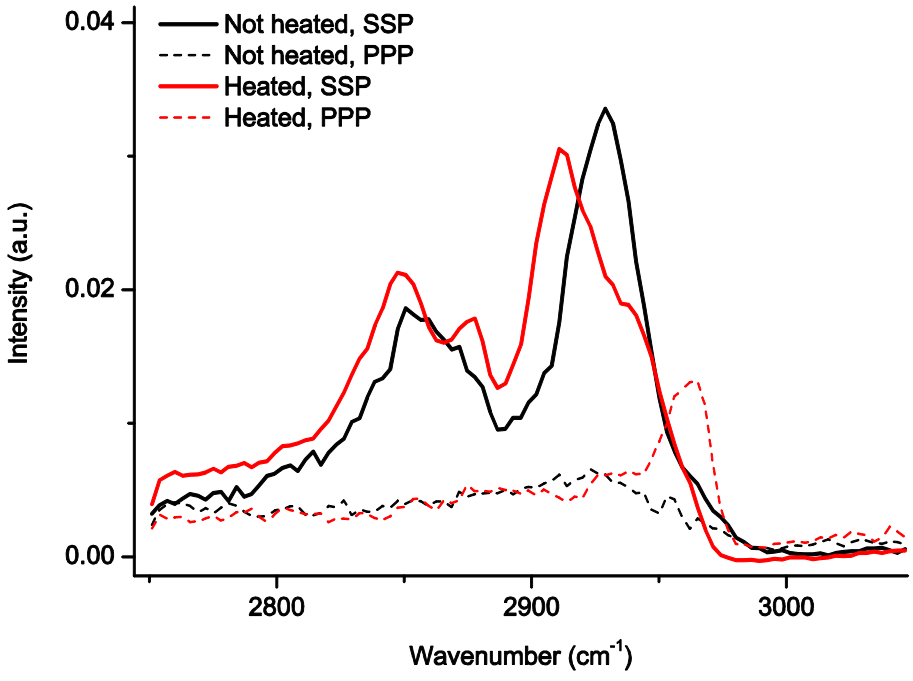

Figure 8. VSF spectra for the SSP and PPP polarization respectively of $(PAH/PAA)_{7.5}$ on glass substrate.

In Figure 8, a CH_2 symmetric stretch can be identified at 2850 cm^{-1} in the SSP polarization of the non-heat-treated sample and its Fermi resonance is visible as a shoulder at around 2920 cm^{-1} [70] These bands originate from the back-bone of the two polyelectrolytes. Also, as the position of the symmetric CH_2 shifts when it is close to a polar group [71], the band centred at

2930 cm^{-1} includes contributions from CH_2 groups located closer to the NH_3 and COOH groups of PAH and PAA respectively [72]. Furthermore, minor additions from weaker bands, such as CH and asymmetric CH_2 cannot be excluded in the region 2875-2920 cm^{-1} [72-74]. The PPP polarized VSF spectrum of the non-heat-treated sample show no visible peaks, which is expected since asymmetric CH_2, although more favourable in the PPP polarization compared with SSP[75], are usually weak due to the fact that the asymmetric CH_2 vibrations have dissimilar frequencies in IR and Raman spectra in general[76]. This has also been observed for e.g. sodium acrylate [77]. The band at 2875 cm^{-1}, visible in the SSP polarization combination for the heat treated sample, corresponds to the symmetric CH_3 stretch, while in the PPP polarization combination the asymmetric CH_3 stretch is seen at 2963 cm^{-1} [70]. The relative strength between the polarization combinations are all in accordance with the so-called polarization rules and supports the assignment [78]. The aforementioned weakness of the asymmetric CH_2 vibrations in VSFS, which otherwise also could have been the origin of this band, also supports this assignment The shoulder appearing at 2940 cm^{-1} in SSP is assigned to the CH_3 Fermi resonance stretching vibration [79] and reside in an environment where the centrosymmetry is broken [80-82]. In a recent VSFS investigation on PEMs made from PAH/PSS, Silva et al. assigned the band at 2875 cm^{-1} to the CH-stretch [83]. However, the CH stretch is seen at around 2890-2900 cm^{-1}, and is usually very weak [73, 84]. Furthermore, the use of different polarization combinations definitely excludes this assignment. Considering the correlation between the increased contact angles, presented in Figure 6, and the increased CH_3 intensity upon heat-treatment, it is concluded that the CH_3 signal originates from the polymer/air interface. VSF spectra of substantially thicker $(PAH/PAA)_{65.5}$ films (results not shown) were similar to those from $(PAH/PAA)_{7.5}$ and supports the fact that the air/polymer interface contributes strongly to the VSF signal.

For the heat-treated sample, a strong peak at 2920 cm^{-1} can also be observed in the VSF spectrum in Figure 8. This may be attributed to CH_2 Fermi resonance, however the reason for its strength upon heat treatment is not known. The decrease seen for the 2930 cm^{-1} peak in SSP, could be due to that polar COO^- and NH_3^+ withdraw from the surface, being hydrophilic groups and thus less energetically favourable at the solid/air interface. This decreases the number of CH_2 close to these groups at the surface and subsequently the VSF signal. The increased intensity of VSFS signals from the methyl groups clearly shows an enrichment of CH_3 groups at the solid/air interface and one interpretation is that this is due to a reorientation of the polymer chain-ends, where the methyl groups are located. Considering the demands for a mode to be VSFS active, it is evident that the CH_3 groups form an ordered structure

Although the results of the VSFS experiments provide a plausible mechanism for the increase in contact angle of the PEMs on flat model surfaces, the discrepancy between the contact angle of the heat treated-sheets and the model surfaces is yet to be explained. However, Zhai et.al [28] have reported an advancing contact angle of 115° for a heat-treated micro-structured LbL film of PAH/PAA, where an acid treatment of a smooth film gave a porous and rough surface (pore size 10 µm and surface roughness >400 nm). Meanwhile the contact angle for water on the flat, non-structured and non-heat-treated conformation was 60°. This suggests that the combination of re-conformation and crosslinking during the heat treatment, together

with the surface roughness which display large similarities to the structure of the fibre network in a paper sheet, creates a hydrophobic surface with the same set of polyelectrolytes used in this work. A similar mechanism has also been suggested by Feng et.al [85] for nanofibers of polyvinyl alcohol (PVA) which are highly hydrophobic as in contrast to a smooth film of the same material. They used angle-resolved XPS to analyze the surfaces and an enrichment of hydrophobic $–CH_2-$ was observed at the solid-air interface compared to the bulk material. The observations are however contradicted by the general view that all highly hydrophobic or superhydrophobic surfaces result from microstructures on a surface with a contact angle originally around 90°. Nevertheless, there is an increasing body of literature reporting that a surface roughness of the appropriate geometry also leads to a highly hydrophobic surface from a previously hydrophilic substrate [85-87]. This has also been theoretically examined by Liu et.al [14], who claim that for certain surface geometries such as mushroom-like microstructures and hierarchical micro- and nano-structures, highly hydrophobic surfaces may be created from hydrophilic substrates. If these theories can be applied to cellulose fiber networks, where it cannot be excluded that such geometries may exist, a combination with the change in surface chemistry as demonstrated by the VSFS measurements is sufficient to create a hydrophobic surface.

4.2 Dry adhesion between cellulose, lignin, and glucomannan model surfaces

Smooth and well-defined wood biopolymer model surfaces were prepared and used in dry adhesion measurements utilizing the JKR technique. For the first time, the elastic hemispherical PDMS cap was surface modified and coated with NFC. This was made through the LbL film assembly of $PAH(NFC/PEI)_{1.5}$ on the cap. Adhesion was measured against flat model surfaces of cellulose (also $PAH(NFC/PEI)_{1.5}$), hemicellulose and lignin.

4.2.1 Model surface characterization

Cellulose I model surfaces were prepared by LbL deposition through dipping of $PAH(NFC/PEI)_{1.5}$ on PDMS caps and flat silicon oxide surfaces. Glucomannan and lignin surfaces were spin coated on silicon oxide substrates. The surface morphologies of typical model surfaces are presented in the AFM images in figure 9a-d. Importantly the $PAH(NFC/PEI)_{1.5}$ resembles a similar dense and smooth fibrillar network on the PDMS and silicon oxide although their rms roughness values differ slightly, 1.7 and 2.7 nm respectively. Some small aggregates could be detected on the glucomannan and lignin films, but these films also showed a low surface roughness of 1.5 and 1.6 nm respectively. These smooth and homogeneous surfaces are a firm prerequisite for fundamental adhesion studies and surface energy determinations using contact angle measurements. The thickness, determined by AFM height scratch analysis, was 40 nm for the spin-coated lignin and glucomannan surfaces and 10 nm for the LbL assembled $PAH(NFC/PEI)_{1.5}$.

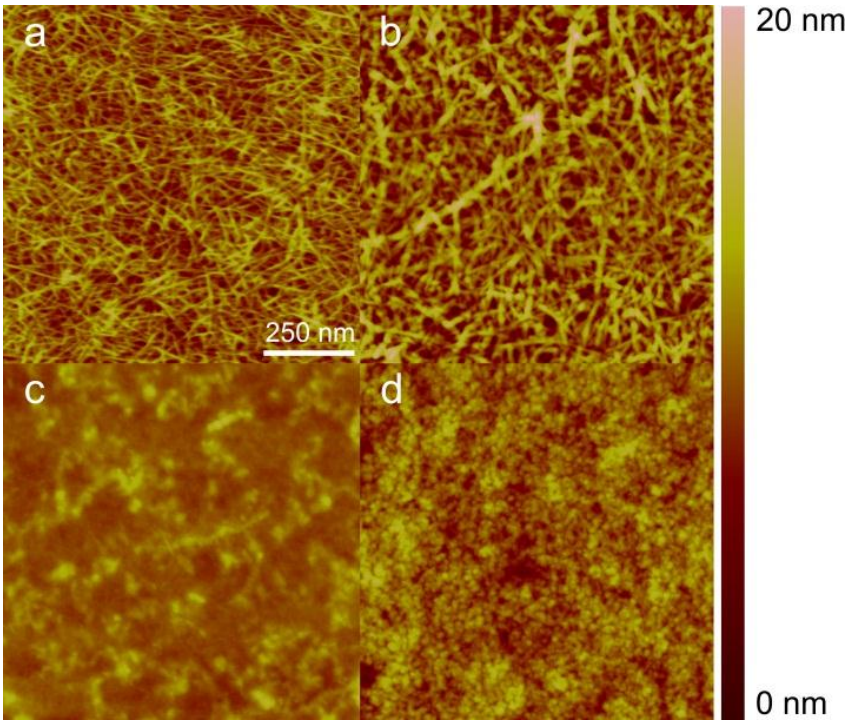

Figure 9. Tapping-mode AFM height images (1 x 1 µm) of wood biopolymer model surfaces: a) PAH(NFC/PEI)$_{1.5}$ on PDMS-cap, b) PAH(NFC/PEI)$_{1.5}$ on flat silica, c) spin-coated glucomannan on flat silica, and d) spin-coated lignin on flat silica.

In addition to the characterization of morphology and thickness, the wood polymer model surfaces, including PAH(NFC/PEI)$_{1.5}$ on flat PDMS, were also characterized in terms of interfacial properties by determining the surface energy through contact angle determinations with water, glycerol and methylene iodine (Table 3).

Table 3. Contact angles of water, glycerol, and methylene iodide on flat wood biopolymer model surfaces

Model surface	Water (deg)	Glycerol (deg)	Methylene iodide (deg)
NFC on SiO2	22	19	34
NFC on PDMS	57	69	67
Glucomannan	19	40	32
Lignin	47	51	37

The total surface energies, as well as their dispersive and polar contributions which provide information about the surface's ability to interact with liquids and other solids, were calculated according to the van Oss method [88]. The results presented in Table 4 indicate that the total surface energies were similar for the model surfaces of all three main wood components. The dispersive component was dominant and almost identical for the three wood biopolymers on SiO_2 substrates, all of which displayed the same surface characteristics, although lignin had a smaller polar component than did the cellulose and glucomannan. The total surface energy and the dispersive component for the PAH(NFC/PEI)$_{1.5}$ on silica were in good agreement with the corresponding values, 58.8 and 40.3 mJm^{-2}, previously reported for

$(PEI/NFC)_1$ on silica [69]. The dispersive component was also similar to the 40-42 mJm^{-2} previously reported for various spin-coated cellulose surfaces [89]. The surface energy of the NFC film on PDMS was substantially lower than that of the NFC film on SiO_2, due mainly to a lower dispersive contribution. Since the morphologies of the $PAH(NFC/PEI)_{1.5}$ films on PDMS and SiO_2 were homogeneous and very similar, the surface energies of $PAH(NFC/PEI)_{1.5}$ were also expected to be similar on the two substrates. However, the film was thinner on the PDMS substrate and if the test liquids can diffuse through the $PAH(NFC/PEI)_{1.5}$ film, the substrate will influence the observed contact angle and thereby the calculated surface energy. The surface energy calculated from the contact angles on $PAH(NFC/PEI)_{1.5}$ on SiO_2 is thus considered to be closer to the actual surface energy of the film.

Table 4. Calculated values for the total surface energy and its components for the wood biopolymer model surfaces.

Model surface	γ^d (mNm/m^2)	γ^+ (mNm/m^2)	γ^- (mNm/m^2)	γ^p (mNm/m^2)	γ^T (mNm/m^2)
NFC SiO_2	42	3.6	18	16	58
NFC PDMS	24	1.4	21	11	35
Glucomannan	43	1.5	30	14	57
Lignin	41	0.7	18	6.9	48

4.2.2 Adhesion measurements

Figures 10a-c show typical graphs of JKR adhesion measurement data from experiments conducted under ambient conditions (25%-35% RH) between cellulose/cellulose, cellulose/glucomannan and cellulose/lignin. The work of adhesion on loading, W_{load} ,and unloading, W_{unload}, were obtained by fitting the data to eq 4. Eq 5 was used to calculate W_{min} from the pull-off force.

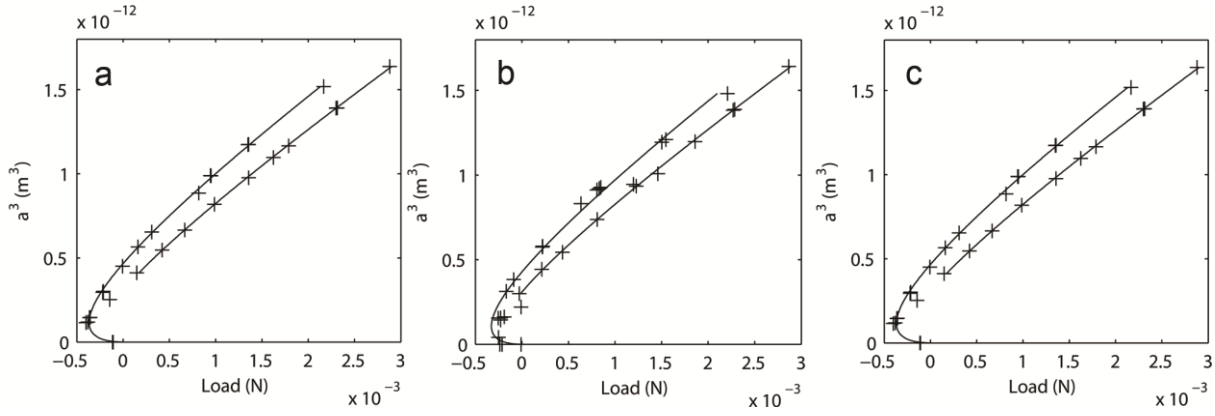

Figure 10. The cube of the contact radius (a^3) as a function of load for a) cellulose/cellulose, b) cellulose/glucomannan, and c) cellulose/lignin. The lines are fitted to the data points according to the inverse of eq 4.

Table 5. Summary of the results from the JKR adhesion measurements for cellulose I–modified PDMS caps, showing the calculated work of adhesion from the loading (W_{load}) and unloading (W_{unload}), the work of adhesion for the pull-off ($W_{pull\text{-}off}$), and the elastic constant of the system (K)

Model surface	W_{load} (mJ m^{-2})	W_{unload} (mJ m^{-2})	$W_{pull\text{-}off}$ (mJ m^{-2})	K (MPa)
NFC	47 ± 4	65 ± 5	59 ± 13	3.4 ± 0.2
Glucomannan	51 ± 5	72 ± 10	62 ± 9	3.5 ± 0.2
Lignin	49 ± 5	63 ± 7	63 ± 13	3.3 ± 0.3

The results of the dry adhesion measurements as presented in Figures 10a-c and Table 5 clearly show that there was no significant difference in the measured adhesion between the investigated systems, i.e. cellulose/cellulose, cellulose/glucomannan and cellulose/lignin. The work of adhesion was approximately 50 mJ m^{-2} for all the systems, and the adhesion hysteresis, i.e. the difference between W_{unload} and W_{load}, was of similar magnitude. These results suggest that the interactions between cellulose, glucomannan and lignin are similar in magnitude and this thereby contradicts the commonly-held view that cellulose is hydrophilic while lignin is hydrophobic. If the architecture of trees and plants is considered, the results in this work are reasonable since a good interaction between the components is a needed to create strong and tough materials.

The surface energies calculated from the contact angle determinations for the model surfaces were used to calculate the work of adhesion, W_{12}, between the model surfaces according to the equation

$$W_{12} = 2\sqrt{\gamma_1^d \gamma_2^d} + 2\left(\sqrt{\gamma_1^+ \gamma_2^-} + \sqrt{\gamma_2^+ \gamma_1^-}\right) \qquad (7)$$

Due to the influence of the substrate on the contact angle determinations on PAH(NFC/PEI)$_{1.5}$ on flat PDMS, the values obtained on the silicon oxide substrate were used when calculating W_{12}. The calculated values of W_{12} were 117 mJ m^{-2}, 117 mJ m^{-2} and 106 mJ m^{-2} for cellulose/cellulose, cellulose/glucomannan and cellulose/lignin respectively.

The calculated W_{12} was similar for all three investigated systems, which supports the conclusion from the JKR measurements that the three wood biopolymers interact well and in a similar fashion with each other. When comparing the calculated W_{12} to the work of adhesion as determined by JKR measurements, it is obvious that the values based on contact angle measurements, although showing the same trends, are significantly larger. The difference can be partly understood by considering what is actually being measured by the two techniques and how the dispersive and polar contributions are affected. The JKR measurements were made under relatively dry conditions (~30% RH) under which dispersive forces are assumed to be dominant. The dispersive part of the calculated surface energy was dominant and very similar for all three model surfaces (Table 4), and this was also reflected in the similarity of the JKR results for the cellulose/cellulose, cellulose/glucomannan and cellulose/lignin systems. Longer contact times in the JKR measurements might have allowed

a reorientation of polymer chains near the interface [90, 91] enabling more polar interactions, even though the mobility of the wood polymers was probably very limited at that low humidity. An important comment is that it is rather well established that the test liquid affects the surfaces in contact angle determinations, leading to a larger measured polar contribution than is actually the case for the dry substrate [92]. This leads to an overestimation of W_{12} when calculated from surface energies.

Although the surface roughness of the model surfaces was very low, it cannot be excluded that the adhesion measured in the JKR measurements was affected. It is well established that surface roughness leads to a lower adhesion due to a decrease in the true contact area, and roughness on the nm level might influence the measurements [93, 94]. Nolte [95] also demonstrated a clear effect of surface roughness when performing JKR adhesion measurement with LbL-coated PDMS caps. Nevertheless, the measurements in the current work show clear trends and suggest that there are no great differences in the adhesive interactions between the investigated wood biopolymers.

5 Conclusions

Fiber modification using PEMs of PAH/PAA and paraffin wax nano-particles resulted in highly hydrophobic paper sheets with a contact angle of 150 °. The adsorption of wax impaired the mechanical properties of the sheets, but at an adsorption of 8 mg wax per gram fiber there was still a 37 % increase in tensile strength index compared to the untreated reference pulp. This demonstrates the flexibility and robustness of the LbL technique in combining the known adhesive effect of (PAH/PAA) with the functionality of the wax nanoparticles, creating a stronger and highly hydrophobic paper.

Without the addition of wax nanoparticles, heat treatment of sheets made of PAH/PAA modified fibers resulted in hydrophobic papers displaying a contact angle for water of 113°. No obvious change in the surface structure was observed, leading to the conclusion that the change in wetting properties was a result of a change in the surface chemistry of the treated fibres. This was further supported by contact angle determinations on PAH/PAA films assembled on well-defined flat cellulose model surfaces, which also exhibited a larger contact angle for water after heat treatment.

Interfacial sensitive Vibrational Sum Frequency Spectroscopy measurements on PAH/PAA films on glass substrates showed that heat treatment resulted in an increased intensity of the CH_3 signals at the solid/air interface. This indicated a heat-induced reorientation of the polymer chain ends, where the methyl groups are located, migrate and reorient towards the interface. Given the hydrophobicity of these groups, it is suggested that a molecular migration and reorientation is the cause of the increase in hydrophobicity on heat treatment.

Successful surface modification of PDMS caps using LbL deposition of NFC and PEI, together with the preparation of smooth homogeneous lignin and glucomannan model surfaces, made it possible to perform the first known all wood biopolymer JKR adhesion measurements, measuring the adhesion between cellulose/cellulose, cellulose/lignin and the cellulose/glucomannan surfaces. The work of adhesion on loading and the adhesion hysteresis were very similar for all three systems, suggesting that the adhesion between the different wood biopolymers does not differ greatly. Compared to adhesion values calculated from the surface energies of the surfaces, obtained from contact angle determinations, the adhesion values from the JKR measurements were lower than expected. Although on different levels, there was nothing contradicting in the trends observed from the two methods, indicating that the mutual adhesive interactions between cellulose/cellulose, cellulose/lignin and cellulose/hemicellulose are on the same level. It is suggested that these differences are caused by an overestimation of the surface energy of the surfaces from the contact angle determinations due to an influence of the liquids on the characterized surfaces and due to a low but nevertheless existing surface roughness of the model surfaces.

The results create a framework for further fundamental JKR adhesion measurements of these systems, where it would be interesting to study the influence of variables such as contact time and humidity as well as chemical and physical modifications of the model surfaces.

6 Acknowledgements

First and foremost I want to thank my supervisor Professor Lars Wågberg for good supervision and for always being positive and enthusiastic.

Lars Ödberg is appreciatively acknowledged for fruitful scientific discussions and support with manuscript writing.

All my co-authors: Erik Johansson, Per Larsson, Jonas Hedberg and Magnus Johnson are thanked for good collaboration.

I would also like to thank all members of the Fibre Technology group and my co-workers at Wallenberg Wood Science Center at KTH for contributing to a fun and creative work environment.

Inga, Mia, Ewa and Mona, thanks for making administrative and practical matters run smoothly.

The Wallenberg Wood Science Center is thanked for financial support.

7 List of abbreviations

AFM	Atomic force microscopy
AKD	Alkyl ketene dimer
CNC	Cellulose nanocrystals
DMSO	Dimethylsulfoxide
DMAc	Dimethyldiacetamine
GGM	Galactoglucomannan
JKR	Johnson-Kendall-Roberts
LbL	Layer-by-layer
NFC	Nanofibrillated cellulose
NMMO	N-methylmorpholine-N-oxide
PAA	Polyacrylic acid
PAH	Polyallylamine hydrochloride
PDMS	Polydimethylsiloxane
PEI	Polyelethylene imine
PEM	Polyelectrolyte multilayers
RH	Relative humidity
Rms	Root mean square
SEM	Scanning electron microscopy
SFA	Surface force apparatus
VSFS	Vibrational sum frequency spectroscopy

8 References

1. Israelachvili, J.N., *Intermolecular and Surface Forces*. FIELD Full Journal Title:1991. 291 pp.
2. Page, D.H., *Theory for the tensile strength of paper.* Tappi, 1969. **52**: p. 674-681.
3. Davison, R.W., *Weak link in paper dry strength.* Tappi, 1972. **55**: p. 567-573.
4. Page, D.H., *The mechanism of strength development of dried pulps by beating.* Svensk Papperstidning, 1985. **88**(3): p. 30-35.
5. Eriksson, M., A. Torgnysdotter, and L. Wågberg, *Surface Modification of Wood Fibers Using the Polyelectrolyte Multilayer Technique: Effects on Fiber Joint and Paper Strength Properties.* Industrial & Engineering Chemistry Research, 2006. **45**(15): p. 5279-5286.
6. Lindström, T., L. Wågberg, and T. Larsson, *On the nature of joint strength in paper - a review of dry and wet strength resins used in paper manufacturing*. Advances in Paper Science and Technology: Transactions of the 13th Fundamental Research Symposium, Vols 1-3, ed. S.J. Ianson2005, Bury: Pulp & Paper Fundamental Research Society. 457-562.
7. Wågberg, L., S. Forsberg, A. Johansson, and P. Juntti, *Engineering of fibre surface properties by application of the polyelectrolyte multilayer concept. Part I. Modification of paper strength.* J. Pulp Pap. Sci., 2002. **28**: p. 222-228.
8. Roberts, J. and Editor, *Paper Chemistry, Second Edition*1996. 320 pp.
9. Von Bahr, M., R. Seppaenen, F. Tiberg, and B. Zhmud, *Dynamic wetting of AKD-sized papers.* Journal of Pulp and Paper Science, 2004. **30**(3): p. 74-81.
10. Werner, O., L. Wagberg, and T. Lindstrom, *Wetting of structured hydrophobic surfaces by water droplets.* Langmuir, 2005. **21**(26): p. 12235-12243.
11. Öner, D. and T.J. McCarthy, *Ultrahydrophobic surfaces. Effects of topography length scales on wettability.* Langmuir, 2000. **16**(20): p. 7777-7782.
12. Nishino, T., M. Meguro, K. Nakamae, M. Matsushita, and Y. Ueda, *The lowest surface free energy based on -CF3 alignment.* Langmuir, 1999. **15**(13): p. 4321-4323.
13. Dorrer, C. and J. Rühe, *Some thoughts on superhydrophobic wetting.* Soft Matter, 2009. **5**(1): p. 51-61.
14. Liu, J.L., X.Q. Feng, G.F. Wang, and S.W. Yu, *Mechanisms of superhydrophobicity on hydrophilic substrates.* Journal of Physics-Condensed Matter, 2007. **19**(35).
15. Decher, G., *Single- and multilayer structures formed on substrates and methods for forming them.* Ger. Offen., 1992: p. 23 pp.
16. Decher, G. and J.B. Schlenoff, eds. *Multilayer Thin Films: Sequential Assembly of Nanocomposite Materials*. 2003, WHILEY-VCH Verlag GmbH & Co.
17. Sun, Y.P., X. Zhang, C.Q. Sun, B. Wang, and J.C. Shen, *Fabrication of ultrathin film containing bienzyme of glucose oxidase and glucoamylase based on electrostatic interaction and its potential application as a maltose sensor.* Macromolecular Chemistry and Physics, 1996. **197**(1): p. 147-153.
18. Westman, E.H., M. Ek, and L. Wagberg, *Antimicrobial activity of polyelectrolyte multilayer-treated cellulose films.* Holzforschung, 2009. **63**(1): p. 33-39.
19. Sukhorukov, G.B., A.A. Antipov, A. Voigt, E. Donath, and H. Mohwald, *pH-controlled macromolecule encapsulation in and release from polyelectrolyte multilayer nanocapsules.* Macromolecular Rapid Communications, 2001. **22**(1): p. 44-46.
20. Eriksson, M., S.M. Notley, and L. Wågberg, *The influence on paper strength properties when building multilayers of weak polyelectrolytes onto wood fibres.* Journal of Colloid and Interface Science, 2005. **292(1)**: p. 38-45.
21. Lingstrom, R., L. Wagberg, and P.T. Larsson, *Formation of polyelectrolyte multilayers on fibres: Influence on wettability and fibre/fibre interaction.* Journal of Colloid and Interface Science, 2006. **296**(2): p. 396-408.
22. Johansson, E., E. Blomberg, R. Lingström, and L. Wågberg, *Adhesive Interaction between Polyelectrolyte Multilayers of Polyallylamine Hydrochloride and Polyacrylic Acid Studied Using Atomic Force Microscopy and Surface Force Apparatus.* Langmuir, 2009. **25**(5): p. 2887-2894.

23. Wågberg, L., G. Decher, M. Norgren, T. Lindström, M. Ankerfors, and K. Axnäs, *The Build-Up of Polyelectrolyte Multilayers of Microfibrillated Cellulose and Cationic Polyelectrolytes.* Langmuir, 2008. **24**(3): p. 784-795.
24. Aulin, C., E. Johansson, L. Wågberg, and T. Lindström, *Self-Organized Films from Cellulose I Nanofibrils Using the Layer-by-Layer Technique.* Biomacromolecules, 2010. **11**(4): p. 872-882.
25. Cranston, E.D. and D.G. Gray, *Morphological and optical characterization of polyelectrolyte multilayers incorporating nanocrystalline cellulose.* Biomacromolecules, 2006. **7**(9): p. 2522-2530.
26. Karabulut, E. and L. Wagberg, *Design and characterization of cellulose nanofibril-based freestanding films prepared by layer-by-layer deposition technique.* Soft Matter, 2011. **7**(7): p. 3467-3474.
27. Glinel, K., M. Prevot, R. Krustev, G.B. Sukhorukov, A.M. Jonas, and H. Moehwald, *Control of the Water Permeability of Polyelectrolyte Multilayers by Deposition of Charged Paraffin Particles.* Langmuir, 2004. **20**(12): p. 4898-4902.
28. Zhai, L., F.C. Cebeci, R.E. Cohen, and M.F. Rubner, *Stable superhydrophobic coatings from polyelectrolyte multilayers.* Nano Letters, 2004. **4**(7): p. 1349-1353.
29. Lingström, R., S.M. Notley, and L. Wågberg, *Wettability changes in the formation of polymeric multilayers on cellulose fibres and their influence on wet adhesion.* Journal of Colloid and Interface Science, 2007. **314**(1): p. 1-9.
30. Yoo, D., S.S. Shiratori, and M.F. Rubner, *Controlling bilayer composition and surface wettability of sequentially adsorbed multilayers of weak polyelectrolytes.* Macromolecules, 1998. **31**(13): p. 4309-4318.
31. Choi, J.Y. and M.F. Rubner, *Selective adsorption of amphiphilic block copolymers on weak polyelectrolyte multilayers.* Journal of Macromolecular Science-Pure and Applied Chemistry, 2001. **38**(12): p. 1191-1206.
32. Israelachvili, J.N. and G.E. Adams, *Measurement of forces between 2 mica surfaces in aqueous electrolyte solutions in range 0-100 nm.* Journal of the Chemical Society-Faraday Transactions I, 1978. **74**: p. 975-&.
33. Ducker, W.A., T.J. Senden, and R.M. Pashley, *Direct measurement of colloidal forces using an atomic force microscope.* Nature, 1991. **353**(6341): p. 239-241.
34. Johnson, K.L., K. Kendall, and A.D. Roberts, *Surface energy and the contact of elastic solid.* Proceedings of the Royal Society of London, Series A: Mathematical, Physical and Engineering Sciences, 1971. **324**(1558): p. 301-13.
35. Chaudhury, M.K. and G.M. Whitesides, *Direct Measurement of Interfacial Interactions between Semispherical Lenses and Flat Sheets of Poly(Dimethylsiloxane) and Their Chemical Derivatives.* Langmuir, 1991. **7**(5): p. 1013-1025.
36. Deruelle, M., L. Leger, and M. Tirrell, *Adhesion at the solid-elastomer interface - influence of the interfacial chains.* Macromolecules, 1995. **28**(22): p. 7419-7428.
37. Norgren, M., S.M. Notley, A. Majtnerova, and G. Gellerstedt, *Smooth model surfaces from lignin derivatives. I. Preparation and characterization.* Langmuir, 2006. **22**(3): p. 1209-1214.
38. Gunnars, S., L. Wågberg, and M.A. Cohen Stuart, *Model films of cellulose: I. Method development and initial results.* Cellulose, 2002. **9**(3): p. 239-249.
39. Eriksson, J., M. Malmsten, F. Tiberg, T.H. Callisen, T. Damhus, and K.S. Johansen, *Enzymatic degradation of model cellulose films.* Journal of Colloid and Interface Science, 2005. **284**(1): p. 99-106.
40. Edgar, C.D. and D.G. Gray, *Smooth model cellulose I surfaces from nanocrystal suspensions.* Cellulose, 2003. **10**(4): p. 299-306.
41. Ahola, S., J. Salmi, L.S. Johansson, J. Laine, and M. Osterberg, *Model films from native cellulose nanofibrils. Preparation, swelling, and surface interactions.* Biomacromolecules, 2008. **9**(4): p. 1273-1282.
42. Aulin, C., I. Varga, P.M. Claesson, L. Wågberg, and T. Lindström, *Buildup of polyelectrolyte multilayers of polyethyleneimine and microfibrillated cellulose studied by in situ dual-polarization interferometry and quartz crystal microbalance with dissipation.* Langmuir, 2008. **24**(6): p. 2509-2518.

43. Holmberg, M., J. Berg, S. Stemme, L. Ödberg, J. Rasmusson, and P. Claesson, *Surface Force Studies of Langmuir-Blodgett Cellulose Films.* Journal of Colloid and Interface Science, 1997. **186**(2): p. 369-381.
44. Rutland, M.W., A. Carambassis, G.A. Willing, and R.D. Neuman, *Surface force measurements between cellulose surfaces using scanning probe microscopy.* Colloids and Surfaces A: Physicochemical and Engineering Aspects. Frontiers in Colloid Chemistry an International Festschrift to Professor Stig E. Friberg, 1997. **123-124**: p. 369-374.
45. Notley, S.M., B. Pettersson, and L. Wågberg, *Direct measurement of attractive van der Waals' forces between regenerated cellulose surfaces in an aqueous environment.* Journal of the American Chemical Society, 2004. **126**(43): p. 13930-13931.
46. Notley, S.M. and M. Norgren, *Surface Energy and Wettability of Spin-Coated Thin Films of Lignin Isolated from Wood.* Langmuir, 2010. **26**(8): p. 5484-5490.
47. Stiernstedt, J., N. Nordgren, L. Wågberg, H. Brumer, III, D.G. Gray, and M.W. Rutland, *Friction and forces between cellulose model surfaces: A comparison.* Journal of Colloid and Interface Science, 2006. **303**(1): p. 117-123.
48. Notley, S.M., M. Eriksson, L. Wågberg, S. Beck, and D.G. Gray, *Surface forces measurements of spin-coated cellulose thin films with different crystallinity.* Langmuir, 2006. **22**(7): p. 3154-3160.
49. Cranston, E.D., D.G. Gray, and M.W. Rutland, *Direct Surface Force Measurements of Polyelectrolyte Multi layer Films Containing Nanocrystalline Cellulose.* Langmuir, 2010. **26**(22): p. 17190-17197.
50. Lee, S.B. and P. Luner, *The wetting and interfacial properties of lignin.* Tappi, 1972. **55**(1): p. 116-121.
51. Tammelin, T., M. Österberg, L.S. Johansson, and J. Laine, *Preparation of lignin and extractive model surfaces by using spincoating technique - Application for QCM-D studies.* Nordic Pulp & Paper Research Journal, 2006. **21**(4): p. 444-450.
52. Timell, T.E., *Recent progress in the chemistry of wood hemicelluloses.* Wood Science and Technology, 1967. **V1**(1): p. 45-70.
53. Nordgren, N., J. Eklöf, Q. Zhou, H. Brumer, and M.W. Rutland, *Top-down grafting of xyloglucan to gold monitored by QCM-D and AFM: Enzymatic activity and interactions with cellulose.* Biomacromolecules, 2008. **9**(3): p. 942-948.
54. Wågberg, L. and R. Hägglund, *Kinetics of polyelectrolyte adsorption on cellulosic fibers.* Langmuir, 2001. **17**: p. 1096-1103.
55. Wågberg, L., L. Winter, L. Ödberg, and T. Lindström, *On the Charge Stoichiometry Upon Adsorption of a Cationic Polyelectrolyte on Cellulosic Materials.* Colloids and Surfaces, 1987. **27**(1-3): p. 163-173.
56. Pääkkö, M., M. Ankerfors, H. Kosonen, A. Nykänen, S. Ahola, M. Österberg, J. Ruokolainen, J. Laine, P.T. Larsson, O. Ikkala, and T. Lindström, *Enzymatic hydrolysis combined with mechanical shearing and high-pressure homogenization for nanoscale cellulose fibrils and strong gels.* Biomacromolecules, 2007. **8**(6): p. 1934-1941.
57. Walecka, J.A., *Low degree of substitution carboxymethylcelluloses.* Tappi FIELD Full Journal Title:Tappi, 1956. **39**: p. 458-63.
58. Norgren, M. and B. Lindstrom, *Dissociation of phenolic groups in kraft lignin at elevated temperatures.* Holzforschung, 2000. **54**(5): p. 519-527.
59. Zhang, Y., J. Li, M.E. Lindström, A. Stepan, and P. Gatenholm. *Spruce glucomannan: Preparation, Purification, Characterization and Derivatization*. in *16th International Symposium on Wood, Fiber and Pulping Chemistry (16th ISWFPC)*. 2011. Tianjin, China.
60. Harris, J.J., P.M. DeRose, and M.L. Bruening, *Synthesis of passivating, nylon-like coatings through cross-linking of ultrathin polyelectrolyte films.* Journal of the American Chemical Society, 1999. **121**(9): p. 1978-1979.
61. Schultz-Eklund, O., C. Fellers, and P.Å. Johansson, *Method for the local determination of the thickness and density of paper.* Nordic Pulp and Paper Research Journal, 1992. **7**: p. 133-9, 154.

62. Johnson, K.L., K. Kendall, and A.D. Roberts, *Surface Energy and the Contact of Elastic Solids.* Proceedings of the Royal Society of London. A. Mathematical and Physical Sciences, 1971. **324**(1558): p. 301-313.
63. Vanoss, C.J., M.K. Chaudhury, and R.J. Good, *Monopolar Surfaces.* Advances in Colloid and Interface Science, 1987. **28**(1): p. 35-64.
64. Della Volpe, C. and S. Siboni, *Some reflections on acid-base solid surface free energy theories.* Journal of Colloid and Interface Science, 1997. **195**(1): p. 121-136.
65. Johnson, C.M., E. Tyrode, S. Baldelli, M.W. Rutland, and C. Leygraf, *A vibrational sum frequency spectroscopy study of the liquid-gas interface of acetic acid-water mixtures: 1. Surface speciation.* Journal Of Physical Chemistry B, 2005. **109**(1): p. 321-328.
66. Zheng, Z.G., J. McDonald, R. Khillan, Y. Su, T. Shutava, G. Grozdits, and Y.M. Lvov, *Layer-by-layer nanocoating of lignocellulose fibers for enhanced paper properties.* Journal of Nanoscience and Nanotechnology, 2006. **6**(3): p. 624-632.
67. Larsson, P.A. and L. Wågberg, *Influence of fibre-fibre joint properties on the dimensional stability of paper.* Cellulose, 2008. **15**(4): p. 515-525.
68. Larsson, P.A. and L. Wagberg, *Diffusion-induced dimensional changes in papers and fibrillar films: influence of hydrophobicity and fibre-wall cross-linking.* Cellulose, 2010. **17**(5): p. 891-901.
69. Aulin, C., S. Ahola, P. Josefsson, T. Nishino, Y. Hirose, M. Österberg, and L. Wågberg, *Nanoscale Cellulose Films with Different Crystallinities and Mesostructures-Their Surface Properties and Interaction with Water.* Langmuir, 2009. **25**(13): p. 7675-7685.
70. Snyder, R.G., H.L. Strauss, and C.A. Elliger, *C-H stretching modes and the structure of normal-aklyl chains.1. long, disordered chains* Journal of Physical Chemistry, 1982. **86**(26): p. 5145-5150.
71. Hsi, S.C., A.P. Tulloch, H.H. Mantsch, and D.G. Cameron, *A vibrational study of the CD2 stretching bands of selectively deuterated palmitic and stearic acids.* Chemistry and Physics of Lipids, 1982. **31**(1): p. 97-103.
72. Murli, C. and Y. Song, *Pressure-Induced Polymerization of Acrylic Acid: A Raman Spectroscopic Study.* The Journal of Physical Chemistry B, 2010. **114**(30): p. 9744-9750.
73. Fox, J.J. and A.E. Martin, *Investigations of Infra-Red Spectra. Determination of C-H Frequencies ($\sim $ 3000 cm.$^{-1} $) in Paraffins and Olefins, with Some Observations on "Polythenes".* Proceedings of the Royal Society of London. Series A. Mathematical and Physical Sciences, 1940. **175**(961): p. 208-233.
74. Lu, R., W. Gan, B.-h. Wu, Z. Zhang, Y. Guo, and H.-f. Wang, *C−H Stretching Vibrations of Methyl, Methylene and Methine Groups at the Vapor/Alcohol (n = 1−8) Interfaces.* The Journal of Physical Chemistry B, 2005. **109**(29): p. 14118-14129.
75. Wang, H.-F., W. Gan, R. Lu, Y. Rao, and B.-H. Wu, *Quantitative spectral and orientational analysis in surface sum frequency generation vibrational spectroscopy (SFG-VS).* International Reviews In Physical Chemistry, 2005. **24**(2): p. 191-256.
76. Tyrode, E. and J. Hedberg, *A Comparative Study of the CD and CH Stretching Spectral Regions of Typical Surfactants Systems Using VSFS: Orientation Analysis of the Terminal CH3 and CD3 Groups.* The Journal of Physical Chemistry C, 2011. **116**(1): p. 1080-1091.
77. Feairheller Jr, W.R. and J.E. Katon, *The vibrational spectra of acrylic acid and sodium acrylate.* Spectrochimica Acta Part A: Molecular Spectroscopy, 1967. **23**(8): p. 2225-2232.
78. Wang, H.F., W. Gan, R. Lu, Y. Rao, and B.H. Wu, *Quantitative spectral and orientational analysis in surface sum frequency generation vibrational spectroscopy (SFG-VS).* International Reviews In Physical Chemistry, 2005. **24**(2): p. 191-256.
79. Snyder, R.G., H.L. Strauss, and C.A. Elliger, *Carbon-hydrogen stretching modes and the structure of n-alkyl chains. 1. Long, disordered chains.* The Journal of Physical Chemistry, 1982. **86**(26): p. 5145-5150.
80. Bain, C.D., *Sum-frequency vibrational spectroscopy of the solid-liquid interface.* Journal of the Chemical Society-Faraday Transactions, 1995. **91**(9): p. 1281-1296.
81. Shen, Y.R., *Optical 2nd harmonic generation at interfaces.* Annual Review of Physical Chemistry, 1989. **40**: p. 327-350.
82. Shen, Y.R., *Surfaces probed by nonlinear optics.* Surface Science, 1994. **299**(1-3): p. 551-562.

83. Silva, H.S. and P.B. Miranda, *Molecular Ordering of Layer-by-Layer Polyelectrolyte Films Studied by Sum-Frequency Vibrational Spectroscopy.* Journal Of Physical Chemistry B, 2009. **113**(30): p. 10068-10071.
84. Lu, R., W. Gan, B.H. Wu, Z. Zhang, Y. Guo, and H.F. Wang, *C-H stretching vibrations of methyl, methylene and methine groups at the vapor/alcohol (n=1-8) interfaces.* Journal Of Physical Chemistry B, 2005. **109**(29): p. 14118-14129.
85. Feng, L., Y.L. Song, J. Zhai, B.Q. Liu, J. Xu, L. Jiang, and D.B. Zhu, *Creation of a superhydrophobic surface from an amphiphilic polymer.* Angewandte Chemie-International Edition, 2003. **42**(7): p. 800-802.
86. Herminghaus, S., *Roughness-induced non-wetting.* Europhysics Letters, 2000. **52**(2): p. 165-170.
87. Zhu, M.F., W.W. Zuo, H. Yu, W. Yang, and Y.M. Chen, *Superhydrophobic surface directly created by electrospinning based on hydrophilic material.* Journal of Materials Science, 2006. **41**(12): p. 3793-3797.
88. Van Oss, C.J., *Interfacial Forces in Aqueous Media*. FIELD Full Journal Title:1994, New York: Marcel Dekker. 432 pp.
89. Eriksson, M., S.M. Notley, and L. Wågberg, *Cellulose Thin Films: Degree of Cellulose Ordering and Its Influence on Adhesion.* Biomacromolecules, 2007. **8**(3): p. 912-919.
90. Choi, G.Y., S.J. Kim, and A. Ulman, *Adhesion hysteresis studies of extracted poly(dimethylsiloxane) using contact mechanics.* Langmuir, 1997. **13**(23): p. 6333-6338.
91. Kim, S.J., G.Y. Choi, A. Ulman, and C. Fleischer, *Effect of chemical functionality on adhesion hysteresis.* Langmuir, 1997. **13**(25): p. 6850-6856.
92. Berg, J.C. and Editor, *Wettability. [In: Surfactant Sci. Ser., 1993; 49]*. FIELD Full Journal Title:1993. 531 pp.
93. Kendall, K., *Molecular Adhesion and Its Applications: The Sticky Universe*2001, New York: Kluwer Academic/Plenum Publishers.
94. Zappone, B., K.J. Rosenberg, and J. Israelachvili, *Role of nanometer roughness on the adhesion and friction of a rough polymer surface and a molecularly smooth mica surface.* Tribology Letters, 2007. **26**(3): p. 191-201.
95. Nolte, A.J., J.Y. Chung, M.L. Walker, and C.M. Stafford, *In situ Adhesion Measurements Utilizing Layer-by-Layer Functionalized Surfaces.* Acs Applied Materials & Interfaces, 2009. **1**(2): p. 373-380.